www.czasopisma.pan.pl PAN www.journals.pan.pl
Opto-Electronics Review 27 (2019) 14–17

Contents lists available at ScienceDirect

Opto-Electronics Review

journal homepage: http://www.journals.elsevier.com/opto-electronics review

Effect of annealing on the structural properties of arsenic-implanted mercury cadmium telluride

I.I. Izhnin[a,b,*], O.I. Fitsych[c], Z. Świątek[d], Y. Morgiel[d], O.Yu. Bonchyk[e], H.V. Savytskyy[e], K.D. Mynbaev[f,g,**], A.V. Voitsekhovskii[b], A.G. Korotaev[b], M.V. Yakushev[h], D.V. Marin[h], V.S. Varavin[h], S.A. Dvoretsky[b,h]

[a] *Scientific Research Company "Electron-Carat", Lviv, 79031, Ukraine*
[b] *National Research Tomsk State University, Tomsk, 634050, Russia*
[c] *Hetman Petro Sahaidachny National Army Academy, Lviv, 79012, Ukraine*
[d] *Institute of Metallurgy and Material Science PAN, Krakow, 30-059, Poland*
[e] *Ya.S. Pidstryhach Institute for Applied Problems of Mechanics and Mathematics NASU, Lviv, 79060, Ukraine*
[f] *Ioffe Institute, Saint–Petersburg, 194021, Russia*
[g] *ITMO University, Saint–Petersburg, 197101, Russia*
[h] *A.V. Rzhanov Institute of Semiconductor Physics, Siberian Branch of the Russian Academy of Sciences, Novosibirsk, 630090, Russia*

ARTICLE INFO

Article history:
Received 30 May 2018
Received in revised form 26 October 2018
Accepted 3 January 2019
Available online 21 January 2019

Keywords:
HgCdTe
Implantation
Defects
Microscopy

ABSTRACT

Effect of annealing on the structural properties of arsenic-implanted mercury cadmium telluride film grown by molecular beam epitaxy was studied with the use of transmission electron microscopy and optical reflection. Strong influence of the graded-gap surface layer grown on top of the film on the behaviour of implantation-induced defects under arsenic activation annealing was revealed and interpreted.

1. Introduction

Mercury cadmium telluride (MCT) has been one of the most important materials in the technology of infrared photodetectors for the last 50 years, and ion implantation remains to be the most common method used for the formation of *p*–*n* junctions for MCT-based photodiodes. Currently, there is a special interest in fabrication of *p*-*n*-junctions based on *n*-type MCT (*n*-base), and the impurity used for producing a p^+-region in an *n*-type material under implantation typically is arsenic [1].

Due to the low energy of the formation of intrinsic defects in MCT, implantation always leads to a significant radiation damage. Irrespective of the valence of the implanted impurity, MCT demonstrates *n*-type conductivity, just because of the donor nature of defects formed as a result of the damage. Fabrication of a p^+–*n*-structure with given electrical parameters requires both elimination of radiation defects and electrical activation of the introduced impurity, and both these goals can be achieved with thermal annealing. Such annealing typically comprises two stages: the first high-temperature but rather short stage activates arsenic as an acceptor and heals most of the radiation damage, while the second stage, performed in saturated mercury vapours at low temperature for ~24 h, annihilates mercury vacancies which were generated at the first stage.

The principal goal of the post-implantation annealing is to achieve desirable electrical/photo-electrical properties of the *p*-*n* junction. This, however, cannot be done without careful consideration for treatment-inflicted changes in the crystal structure of the material. This is why the microstructure of implanted MCT has been a subject of thorough investigation with the use of various methods, including electron microscopy [2–5]. The purpose of this work was to study the structural properties of arsenic-implanted MCT both before and after post-implantation annealing. For the study, we used electron microscopy and optical reflection, so information on both the surface of the material and on the implanted/damaged layer(s) lying beneath the surface could be obtained.

* Corresponding author at: Scientific Research Company "Electron-Carat", Lviv, 79031, Ukraine
** Corresponding author at: Ioffe Institute, Saint–Petersburg, 194021, Russia
E-mail addresses: i.izhnin@carat.electron.ua (I.I. Izhnin), mynkad@mail.ioffe.ru (K.D. Mynbaev).

https://doi.org/10.1016/j.opelre.2019.01.002
1230-3402/

2. Materials and methods

Studied were samples cut from an MCT epitaxial film grown at Rzhanov Institute of Semiconductor Physics (Novosibirsk, Russia) by molecular-beam epitaxy (MBE) on a (013) CdTe/ZnTe/Si substrate [6]. The 'working' layer of the film had constant chemical composition (CdTe molar fraction) x = 0.22. On top of this layer, a graded-gap protective surface layer was grown in situ. The chemical composition at the surface of this layer approached x = 0.46, the thickness of the layer was of ~400 nm. The total thickness of the film was of 9.1 μm. During the growth, it was doped with indium (donor in MCT) with a concentration of $\sim 5 \cdot 10^{15}$ cm^{-3}. This resulted in *n*–type conductivity with electron concentration and mobility, as established with the Hall-effect measurements at 77 K, $3.9 \cdot 10^{14}$ cm^{-3} and $\mu_n = 87{,}500$ cm^2/(V·s), respectively. Samples were implanted with As$^+$ ions with energy 190 keV and fluences 10^{14} cm^{-2} and 10^{15} cm^{-2}. The implantation was performed with the use of IMC200 (Ion Beam Services, France) system. After the implantation, samples were subjected to a two-stage thermal activation annealing in saturated mercury vapours (360 °C, 2 h and 220 °C, 24 h).

Arsenic secondary-ion mass-spectroscopy (SIMS) profiles were recorded using Cameca IMS-6 F machine with As detection limit $\sim 1 \cdot 10^{16}$ cm^{-3}. The microstructure of the samples was studied with the use of Transmission Electron Microscopy (TEM) in bright-field (BF) mode with the use of a Tecnai G2 F20, FEI Company microscope. TEM lamellas were prepared with the use of FEI Quanta 200 dual beam focused ion beam machine equipped with Omniprobe^{TM} lift-out system. The sample was first covered with a 300 nm amorphous carbon layer. This prevented the surface from the damage that could be inflicted by Ga$^+$ ions used for deposition of a platinum bar used later for lifting the lamella, and helped to elucidate surface details at the light carbon background. The damage from Ga$^+$ ions was further minimized by limiting the gallium beam current during cutting side trenches (starting from 20 nA, through 7 nA and finishing with 5 nA) and final polishing of the lifted lamella (starting from 1 nA, through 0.3 nA and finishing with 0.1 nA).

Structural properties of the surface of the samples were accessed with optical reflection studies performed at 300 K. The reflection spectra were recorded in the wavelength range 300–800 nm with the 0.2 nm step using a Shimadzu UV-3600 spectrometer.

3. Results and discussion

Figure 1 shows SIMS profiles for the studied samples along with similar data from the literature. According to our SIMS data, the implanted arsenic ions could be traced to the depth of ~400 nm and, thus. were located within the graded-gap protective surface layer. Curve *1* shows SIMS profile for the sample which was implanted with the energy of 190 keV and the fluence of 10^{14} cm^{-2}. In this sample the graded-gap surface layer remained intact. The projected ion range R_p corresponding to maximum arsenic concentration was of ~95 nm. Curves *2* and *3* show profiles for the samples implanted with the energy of 190 keV and the fluence of 10^{15} cm^{-2}, here implantation was performed both in the sample with the graded-gap surface layer (curve *2*) and after this layer was removed chemically (curve *3*). By comparing curves *2* and *3* in Fig. 1 one can conclude that the graded-gap surface layer hardly had any effect on the arsenic distribution profile. Shi, *et al.* [5] presented results of arsenic implantation in MCT performed through ZnS or CdTe capping layers, and showed that it was a type of structure (columnar or layered) of the capping layer that defined the penetration depth of implanted atoms. Thus, as our graded-gap surface layer was grown in situ and repeated the crystal structure of the 'working' layer, the similarity between curves *2* and *3* in Fig. 1 is understandable. Curves *4* and *5* show SIMS profiles recorded by Mollard, *et al.* [4] for MCT grown on a CdZnTe substrate and implanted with arsenic with 180 keV energy and fluences of $2 \cdot 10^{14}$ cm^{-2} (curve *4*) and $2 \cdot 10^{15}$ cm^{-2} (curve *5*). It can be seen that the shape of curve *4* repeats that of curve *1*, but arsenic concentration at the same depth for the former is slightly higher. Arsenic concentration of 10^{20} cm^{-3} in the maximum of the profile was achieved by Mollard, *et al.* [4] for the ion fluence of $2 \cdot 10^{15}$ cm^{-2} (curve *5*). Except for the top surface layer (50–100 nm), profiles *2*, *3* and *5* for samples implanted with a $\sim 10^{15}$ cm^{-2} fluence look very similar.

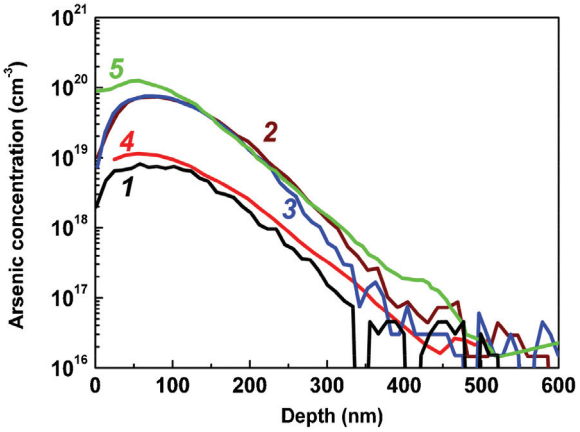

Fig. 1. Arsenic profiles in MBE-grown MCT recorded with SIMS: curve *1*, 190 keV energy and $1 \cdot 10^{14}$ cm^{-2} fluence (this work, Si substrate and graded-gap surface layer intact); curve *2*, 190 keV and $1 \cdot 10^{15}$ cm^{-2} (this work, Si substrate and graded-gap surface layer intact); curve *3*, 190 keV and $1 \cdot 10^{15}$ cm^{-2} (this work, Si substrate and graded-gap surface layer removed); curve *4*, 180 keV and $2 \cdot 10^{14}$ cm^{-2}, and curve *5*, 180 keV and $2 \cdot 10^{15}$ cm^{-2}, CdZnTe substrate, after Ref. [4].

Figure 2 shows BF TEM images of a cross-section of the sub-surface area of arsenic-implanted (Fig. 2a) and implanted and annealed (Fig. 2b) samples. Images shown for the samples implanted with a 190 keV energy and a 10^{14} cm^{-2} fluence. Comparing Figs. 1 and 2, one can conclude that the radiation damage extended much deeper than the projected ion range. This is typical of the materials with strong ionicity of chemical bonds, including II–VI semiconductors in general, and MCT, in particular [4]. The defect pattern observed in Fig. 2a is typical of arsenic-implanted MCT in a sense that a number of defect layers with different thicknesses *d* and types and concentrations of defects is observed (see, e.g., [2–5]). In particular, the top surface layer (d ~50 nm) contains, according to BF TEM data, very few defects, if at all. The next, sub-surface, layer (d ~120 nm), contains large extended defects with high density, and the deep defect layer (d ~80 nm), smaller defects with moderate density. TEM studies in high-resolution mode performed on similar samples allowed for identifying dominant defects as dislocations, defect clusters, stacking faults and nano-twins (top layer), large-size dislocation loops (middle layer), and smaller-size dislocation loops (lower layer) [7].

A defect pattern presented in TEM image in Fig. 2b is different from that in Fig. 2a. In Fig. 2b one can also distinguish three defect layers, but their structure and thicknesses strongly differ from those in Fig. 2a. In particular, the top 'low-defect' layer now has only 10 nm in thickness, 'middle-layer' (d ~60 nm) contains dislocations with very high density, and deep layer (d ~170 nm), dislocation loops with the moderate density, which is decreasing towards the depth of the sample.

Figure 3 shows optical reflection spectra of the sample implanted with the energy of 190 keV and the fluence of 10^{14} cm^{-2}. To test the effect of arsenic activation annealing on the structure of non-implanted MCT, a piece of as-grown film was also annealed in this regime without implantation. The spectra shown in Fig. 3 cor-

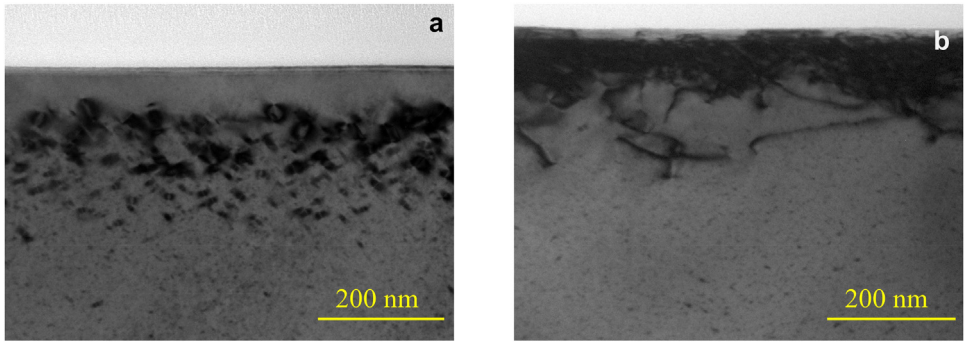

Fig. 2. Cross-sectional BF TEM images of the sub-surface area in MCT sample implanted with arsenic (190 keV energy and 10^{14} cm^{-2} fluence) before (a) and after (b) activation annealing.

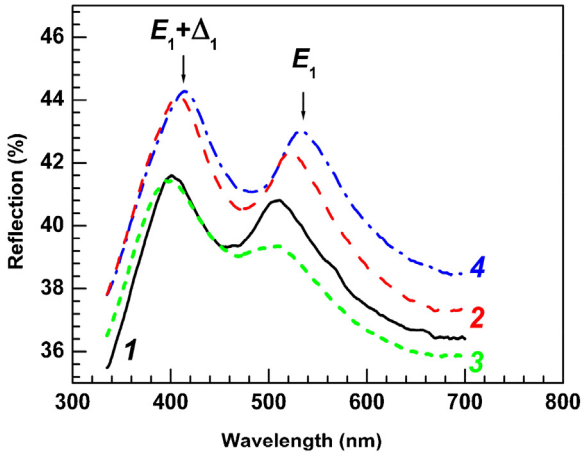

Fig. 3. Optical reflection spectra of an MCT sample implanted with arsenic ions with the energy of 190 keV and the fluence of 10^{14} cm^{-2}: after the growth (*1*); after activation annealing performed on the as-grown sample without ion implantation (*2*); after ion implantation into as-grown sample (*3*); after activation annealing of the implanted sample (*4*).

respond to: the initial (as-grown) film (spectrum *1*), a sample after activation annealing without implantation (*2*), a sample straight after ion implantation (*3*), and an implanted and annealed sample (*4*). For all the spectra, two distinct peaks were observed, a characteristic doublet of peaks E_1 and $E_1+\Delta_1$ which originate in transitions $\Lambda_{4,5} \rightarrow \Lambda_6$ and $\Lambda_6 \rightarrow \Lambda_6$ [8,9]. It is believed that the energy position and the shape of the peaks give information on the value of energy gap (and, correspondingly, chemical composition) of MCT and structural perfection of the material, respectively. To assess the change in the shape of the peaks after the treatments, we used the value of ṗeak sharpness¨ $Q = \Delta R/R_1$, where ΔR is the value of the 'dip' between the peaks and R_1 is the reflection in the maximum of the peak E_1 [10]. For the as-grown film (curve *1*), the sharpness parameter of the E_1 peak was $Q = 4.55$. Sample after activation-type annealing (without implantation) had $Q = 6.02$ (curve *2*), which showed that the annealing resulted in some ordering of MCT crystal structure. This can be possibly related to partial annealing of stacking faults typical of MCT grown on silicon substrate [6]. Also, a **red-**shift of the maxima of curve *2* in respect to that of curve *1* is indicative of some decrease of x at the surface of the film, possibly due to diffusion of Cd and Hg. After ion implantation (curve *3*) the sharpness decreased to $Q = 2.58$, which was indicative of a strong damage to an MCT lattice in the surface region. After activation annealing of the implanted film (curve *4*), Q increased to 5.62, which was higher than that in the as-grown film and close to Q for the film annealed immediately after the growth. This seemed to indicate almost complete annealing of the implantation-inflicted structural defects on the surface. A beneficial effect of activation annealing on the structural perfection of the surface of implanted MCT was also demonstrated in other optical reflection experiments [11]. Obviously, quality of the surface is very important, as it ensures the smoothness of device processing, as well as the stability of the parameters of photodiodes during their lifetime.

Thus, speaking of the surface and sub-surface region, after the annealing we observed two major features: *i*) transformation of dislocation loops into single dislocations with high density and thinning of the surface 'defect-free' layer along with the general 'movement' of defect layers towards the surface (according to TEM data), and *ii*) improvement in crystal quality of the surface (according to optical reflection data). Considering that under conditions used, visible radiation penetrates MCT not deeper than 50 nm [9], it can be concluded that region containing single dislocations, even with high density, structurally appeared to be more perfect than that with dislocation loops with average density.

Observation of a 'low-defect' surface layer on the surface of the implanted material and its thinning after annealing represents an interesting phenomenon. For example, this layer was not observed in similar MBE-grown MCT structures with removed graded-gap surface layer implanted with arsenic with a 10^{15} cm^{-2} fluence and a 190 keV energy [11]. However, Lobre *et al.* [2] for liquid-phase epitaxy (LPE)–grown homogeneous MCT film implanted with arsenic with a 360 keV energy and low fluence ($5{\cdot}10^{13}$ cm^{-2}) observed a shallow zone with few defects with the depth of about 40 nm under the surface, though for a $2{\cdot}10^{14}$ cm^{-2} fluence such zone was not detected. This does not allow for relating the 'low-defect' layer purely to the existence of the graded-gap surface layer, but rather to the ion dose used, perhaps, in combination with ion energy. In Refs. 2–4, after a single-step high temperature (420 °C) annealing under Hg overpressure, the TEM images appeared to be almost clear of dislocations. Mollard, *et al.* [4] noted that even low-temperature (200 °C) annealing resulted in drastic decease in dislocation density. However, the evolution of defects as a result of the annealing was different to that observed in this work: in Ref. 4 dislocations below the surface grew in size and reduced their density, while the smaller defects evolved into dislocation loops. Increasing the annealing temperature up to 300 °C, according to Ref. 4, led to long dislocations increasing in size, while small dislocation loops, lying deeper in the material, showed a tendency to disappear. In general, Mollard *et al.* [4] concluded that 'when increasing the temperature for the same annealing time, dislocation loops grow in size due to the accumulation of single defects. As a consequence of that, it could be expected that their density would decrease, while their size would increase. We can suggest that this process is similar to coarsening which describes structural evolution proceeding when in a multi-phase system larger objects grow at the expense of smaller ones to reduce the total free energy of the system. The

presence (or absence) of a free surface is an important aspect of this effect, as transformation of dislocations and dislocation loops (as well as smaller defect clusters and complexes) is driven by diffusion of vacancies and much more movable mercury interstitials, which typically constitute these defects [4]. Interestingly, that according to Shi, *et al.* [5], the presence of uniform CdTe capping layer did not hinder neither healing of structural damage nor effective diffusion of implanted arsenic atoms after post-implantation annealing in LPE– and MBE–grown MCT. It is known, however, that the graded-gap surface layer strongly intervenes with diffusion and general defect behaviour via its built-in electric field, which was demonstrated for both ion–implanted and ion–milled MCT [12]. Thus, the difference between TEM results obtained after post-implantation annealing in this work and in Refs. 2–5 can be indeed attributed to the effect of the graded-gap surface layer. It seems that the whole 'movement' of defect layers towards the surface as a result of annealing is very much driven by its influence.

4. Conclusions

In conclusion, the effect of annealing on the structural properties of arsenic-implanted HgCdTe film with a graded-gap surface layer was studied with the use of transmission electron microscopy and optical reflection. No influence of the graded-gap layer was found on the distribution of arsenic in as-implanted samples. At the same time this layer appeared to strongly affect the re-structuring of the radiation-damaged material during post-implantation annealing via the influence on the diffusion of point defects. The structural perfection of the surface after the annealing appeared to be high, yet a defect area with high density of single dislocations was found under the surface of the material. After the annealing the whole 'defect' layer appeared to be shifted to the surface of MCT.

References

[1] W. Lei, J. Antoszewski, L. Faraone, Progress, challenges, and opportunities for HgCdTe infrared materials and detectors, Appl. Phys. Rev. 2 (2015), 041303.
[2] C. Lobre, P.H. Jouneau, L. Mollard, P. Ballet, Characterization of the microstructure of HgCdTe with *p*-type doping, J. Electron. Mater. 43 (2014) 2908–2914.
[3] L. Mollard, G. Destefanis, N. Baier, J. Rothman, P. Ballet, J.P. Zanatta, M. Tchagaspanian, A.M. Papon, G. Bourgeois, J.P. Barnes, C. Pautet, P. Fougeres, Planar *p*-on-*n* HgCdTe FPAs by arsenic ion implantation, J. Electron. Mater. 38 (2009) 1805–1813.
[4] L. Mollard, G. Destefanis, G. Bourgeois, A. Ferron, N. Baier, O. Gravrand, J.P. Barnes, A.M. Papon, F. Milesi, A. Kerlain, L. Rubaldo, Status of *p*-on-*n* arsenic-implanted HgCdTe technologies, J. Electron. Mater. 40 (2011) 1830–1839.
[5] C.Z. Shi, C. Lin, Y.F. Wei, L. Chen, M. Zhu, Barrier layer induced channeling effect of As ion implantation in HgCdTe and its influences on electrical properties of *p*–*n* junctions, Appl. Optics 55 (2016) D101–D105.
[6] M.V. Yakushev, A.K. Gutakovsky, I.V. Sabinina, Yu.G. Sidorov, Defects in the crystal structure of $Cd_xHg_{1-x}Te$ layers grown on the Si (310) substrates, Semiconductors 45 (2011) 926–934.
[7] O.Yu Bonchyk, H.V. Savytskyy, Z. Swiatek, Y. Morgiel, I.I. Izhnin, A.V. Voitsekhovskii, A.G. Korotaev, K.D. Mynbaev, O.I. Fitsych, V.S. Varavin, S.A. Dvoretsky, D.V. Marin, M.V. Yakushev, Nano-size defects in arsenic-implanted HgCdTe films: a HRTEM study, Appl. Nanosci. (2019), http://dx.doi.org/10.1007/s13204-018-0679-y, in press.
[8] H. Arwin, D.E. Aspnes, Nondestructive analysis of $Hg_{1-x}Cd_xTe$ (x=0.00, 0.20, 0.29, and 1.00) by spectroscopic ellipsometry. II. Substrate, oxide and interface properties, J. Vac. Sci. Technol. A 2 (1984) 1316–1323.
[9] P. Koppel, Visible and ultraviolet reflectivity of $Hg_{1-x}Cd_xTe$, J. Appl. Phys. 57 (1985) 1705–1709.
[10] S.A. Dvoretsky, N.N. Mikhailov, V.G. Remesnik, N.Kh. Talipov, Using reflection spectroscopy for assessing structural perfection of CdTe/GaAs films and $Cd_xHg_{1-x}Te$ crystals, Avtometriya 5 (1998) 73–77, in Russian.
[11] I.I. Izhnin, E.I. Fitsych, A.V. Voitsekhovskii, A.G. Korotaev, K.D. Mynbaev, V.S. Varavin, S.A. Dvoretsky, N.N. Mikhailov, M.V. Yakushev, A.Yu. Bonchyk, H.V. Savytskyy, Z. Świątek, Defects in arsenic-implanted p^+–*n*- and n^+–*p*-structures based on MBE-grown CdHgTe films, Russ. Phys. J. 60 (2018) 1752–1757.
[12] O.I. Fitsych, A.V. Voitsekhovskii, D.V. Grigorjev, N.N. Mikhailov, N.H. Talipov, K.D. Mynbaev, I.I. Izhnin, Ion implantation and ion milling in MBE $Hg_{1-x}Cd_xTe$ films, Nucl. Instrum. Methods Phys. Res. B 272 (2012) 313–317.